

Exploring compactified HEIDI models at the LHC

Neil D. Christensen,^{1,*} Benjamin Fuks,^{2,†} Jürgen Reuter,^{3,‡} and Christian Speckner^{4,§}

¹ *PITTSburgh Particle physics, Astrophysics and Cosmology Center,
Department of Physics and Astronomy, University of Pittsburgh,
Pittsburgh, PA 15260, USA*

² *Institut Pluridisciplinaire Hubert Curien/Département Recherche Subatomique
Université de Strasbourg/CNRS-IN2P3
23 Rue du Loess, F-67037 Strasbourg, France*

³ *DESY, Theory Group, Bldg. 2a, Notkestr. 85, D-22603 Hamburg, Germany*

⁴ *Albert-Ludwigs-Universität Freiburg, Physikalisches Institut
Hermann-Herder-Straße 3, 79104 Freiburg, Germany*

Abstract

Models with multi-scalar Higgs sectors inspired by a higher-dimensional setup are interesting alternatives to the Standard Model because, although they have a Higgs sector which gives mass to the W and Z gauge bosons as well as the SM fermions, this Higgs sector is potentially undiscoverable at the Large Hadron Collider or shows considerable deviations from the Standard Model Higgs sector. We investigate a compactified version of such models and study its phenomenology in the “golden” four-lepton channel at the LHC in areas of parameter space compatible with electroweak precision observables .

*neilc@pitt.edu

†benjamin.fuks@iphc.cnrs.fr

‡juergen.reuter@desy.de

§christian.speckner@physik.uni-freiburg.de

I. INTRODUCTION

The Standard Model (SM) of particle physics provides a successful description of all experimental high-energy data to date. However, despite its success, many fundamental questions remain unanswered, such as the origin of electroweak symmetry breaking, the nature of neutrino masses, the large hierarchy between the electroweak and the Planck scales and the origins of dark matter and the cosmological constant. Attempts to address these questions have led to a wide range of new physics theories, most of them predicting new phenomena at the TeV scale. The Large Hadron Collider (LHC) at CERN is currently probing this scale and will hopefully make it possible to discover, constrain and/or exclude some of the proposed theories beyond the Standard Model (BSM).

The Higgs boson as the last piece of the SM has been searched for over several decades now. After the unsuccessful search for it at the LEP e^+e^- collider as well as the Tevatron (though there are some hints in a slight excess now in a broad mass range from 120-140 GeV) several models that explain electroweak symmetry breaking (EWSB) as well as unitarization of tree level scattering amplitudes have been constructed that either work without a scalar state being present or sport invisible or undetectable decays of those states. One type of these models are the so-called HEIDI models [1–3] (an onomatopoeic version of the acronym for higher dimensions), based on an older model presented in [5]. The basic idea of this class of models is that the Higgs field mixes with a certain number of inert (singlet) fields, the number of which can be increased until they become a continuum. This admixture with such a set or continuum of fields can distort the properties of the physical Higgs particle(s), i.e. its production cross sections, its decay width and branching ratios. At the moment, there seems to be some evidence for a SM-like Higgs boson around 125 GeV, which could have modified couplings to SM particles, as the diphoton rate seems to be rather enhanced, while the WW^* decay seems to be suppressed with respect to the SM. Recently, the aforementioned models have been modified in order to precisely explain these deviations from the SM values [4].

An interesting feature of this type of model is that it may hide the source of electroweak symmetry breaking from discovery at the LHC. We know that, if the electroweak symmetry is broken explicitly in the Lagrangian (rather than through an asymmetric vacuum), the scattering of longitudinal electroweak vector bosons grows quadratically with energy and exceeds the perturbative unitarity bound at just over a TeV. As a result, we know that some new physics must appear below that scale in order to unitarize the theory. The common assumption is that we cannot fail to discover this new physics at the LHC. HEIDI type models, however, have areas of parameter space which are consistent with precision constraints, but may have such a broad signal as to be undetectable at the LHC with current methods [1, 2].

In this work we will be examining a HEIDI type model which includes an infinite but discrete set of additional scalar resonances. The model is realized by means of a spatial and compact extra dimension with the SM being confined to a four-dimensional brane within the five-dimensional spacetime. The only field which is allowed to propagate into the bulk of the extra dimension is a singlet scalar field coupled to the scalar sector of the SM through a trilinear coupling. After Kaluza-Klein (KK) reduction, we obtain an infinite number of new scalar fields mixing with the SM Higgs boson. Depending on the point in the parameter space, many KK states could be well below the TeV scale, and the emerging collider phenomenology of the scalar sector can thus be very different from the SM. In

order to assess the impact of the modified scalar sector on the Higgs searches, we study the so-called golden channel gluon fusion process.

The outline of this paper is as follows: in Sec. II we present our class of HEIDI models including their Lagrangian and derive the mass eigenvalues and eigenstates of the scalar sector together with its couplings to the SM particles. We discuss the parameter space of HEIDI models and examine different characteristic incarnations of the scalar sector depending on the hierarchies in the parameter space. The simulation of such models is potentially very demanding as the number of physical particles in the spectrum can be very large and depends on the point in parameter space, and our way of tackling these technical difficulties is discussed in Sec. III. In Sec. IV, our results for the golden channel of a Higgs boson decaying into ZZ^* into four leptons at the LHC are shown, which is (if the Higgs mass is not too close to the LEP limit) the cleanest and most background-free channel. Finally, we conclude.

II. THE MODEL

A. Lagrangian and spectrum

The compact HEIDI model discussed in this paper is a representative of the class of models suggested in Ref. [1]. The model is a renormalizable extension of the Standard Model formulated on Minkowski spacetime plus an additional spatial extra dimension compactified on a circle with radius R and denoted in the following by the coordinate y . In this model the Standard Model is confined to the $y = 0$ brane, with the Higgs sector supplemented by an additional scalar gauge-singlet field $\Omega(x, y)$ which is the only field allowed to propagate in the bulk of the extra dimension. The action of the scalar sector is chosen¹ to be

$$S = \underbrace{\int d^4x \left(\frac{1}{2} (D_\mu \Phi)^\dagger D^\mu \Phi + \frac{\mu^2}{2} \Phi^\dagger \Phi - \frac{\lambda}{4} (\Phi^\dagger \Phi)^2 \right)}_{S_\Phi} + \underbrace{\int d^4x \int_0^{2\pi R} dy \left(\frac{1}{2} \partial_a \Omega \partial^a \Omega - \frac{m_b^2}{2} \Omega^2 + g \Phi^\dagger \Phi \Omega \delta(y) \right)}_{S_\Omega}, \quad (1)$$

with Φ being the Standard Model Higgs doublet (for later convenience we use a non-canonical normalization of Φ) and S_Φ the action describing the SM Higgs sector. From Eq. (1), it is evident that the only difference with respect to the SM is the additional sector S_Ω , which contains a trilinear coupling g between the Higgs field and the new scalar singlet Ω .

In order to work out the equivalent four-dimensional theory, we decompose the new scalar field in terms of its KK excitations²

$$\Omega(x, y) = \sum_{k=0}^{\infty} \frac{1}{N_k \sqrt{R}} \Omega_k(x) \cos \frac{k}{R} y, \quad \text{with} \quad N_k = \sqrt{(1 + \delta_{k0}) \pi}. \quad (2)$$

¹ We omit any self-interactions of Ω in the same spirit as Ref. [1] as they would spoil renormalizability.

² The sine modes in the KK decomposition decouple from the SM, so we omit them.

Inserting Eq. (2) into Eq. (1), we obtain the four-dimensional action

$$S_\Omega = \int d^4x \sum_{k=0}^{\infty} \left(\frac{1}{2} \partial_\mu \Omega_k \partial^\mu \Omega_k - \frac{1}{2} m_k^2 \Omega_k^2 + \frac{g}{N_k \sqrt{R}} \Phi^\dagger \Phi \Omega_k \right) , \quad (3)$$

where the masses of the KK modes are given by

$$m_k^2 = m_b^2 + \frac{k^2}{R^2} .$$

Like in the SM, spontaneous symmetry breaking occurs if $\mu^2 > 0$ (see Appendix A 1 for a detailed discussion of the potential and the vacuum expectation values). Rotating to unitarity gauge and shifting the scalar fields by their vacuum expectation values (vev), we get

$$\Phi(x)_{\text{unit.}} = \begin{pmatrix} 0 \\ v + h(x) \end{pmatrix} , \quad \Omega_k(x) = w_k + \omega_k(x) , \quad (4)$$

where the vevs are given by

$$v = \frac{\mu}{\sqrt{\lambda - \alpha}} \left(\text{with } \alpha = \frac{g^2}{m_b} \coth(m_b R \pi) \right) , \quad w_k = \frac{g v^2}{\sqrt{R} N_k m_k^2} . \quad (5)$$

Defining the Higgs mass in the usual way,

$$m_h = \sqrt{2\lambda} v , \quad (6)$$

the four-dimensional Lagrangian for the scalar fields, expanded around the correct vacuum, reads

$$\begin{aligned} \mathcal{L}_{\text{scalar}} = & \frac{1}{2} \partial^\mu h \partial_\mu h - \frac{1}{2} m_h^2 h^2 - \lambda v h^3 - \frac{\lambda}{4} h^4 \\ & + \sum_{k=0}^{\infty} \left(\frac{1}{2} \partial_\mu \omega_k \partial^\mu \omega_k - \frac{1}{2} m_k^2 \omega_k^2 + \frac{2g v}{N_k \sqrt{R}} h \omega_k + \frac{g}{N_k \sqrt{R}} h^2 \omega_k \right) . \end{aligned} \quad (7)$$

In the equation above, we have omitted constant terms as well as all the terms involving gauge bosons included in the covariant derivative of Eq. (1) (which are unchanged with respect to the SM). Note that Eq. (5) implies a condition on the quartic Higgs coupling λ , the trilinear coupling g^2 , the bulk mass m_b and the compactification scale R^{-1} ,

$$\lambda > \alpha = \frac{g^2}{m_b} \coth(m_b R \pi) . \quad (8)$$

As shown in Appendix A 1, violation of Eq. (8) leads to an unstable theory with a potential which is not bounded from below³.

Owing to the trilinear coupling between Φ and Ω in the original action, Eq. (7) contains a mixing between h and the ω_k which therefore do not correspond to mass eigenstates. While

³ With the exception $\lambda = \alpha$ and $\mu^2 < 0$, in which case the potential is bounded and has a single minimum at $v = w_k = 0$.

this mixing is resummed to obtain an effective Higgs propagator in Ref. [1], we here take a different approach and diagonalize the mass matrix explicitly. This calculation leads to the mass eigenvalues λ_k as the zeroes of a transcendental function (see Appendix A 2 for details),

$$f(\lambda_k^2) = m_h^2 + \frac{2g^2v^2}{\sqrt{\lambda_k^2 - m_b^2}} \cot \left(R\pi\sqrt{\lambda_k^2 - m_b^2} \right) - \lambda_k^2 = 0 . \quad (9)$$

It is easy to see from monotony arguments that the spectrum consists of exactly one mode λ_k^2 in each interval

$$m_b^2 + \frac{(k-1)^2}{R^2} < \lambda_k^2 < m_b^2 + \frac{k^2}{R^2} \quad \text{with} \quad k \geq 1 , \quad (10)$$

as well as an additional mode λ_0^2 below m_b^2 .

B. SM couplings and parameter space

The mass eigenstates ϕ_k belonging to the mass eigenvalues λ_k^2 are linear combinations of the fields h and ω_k ,

$$\phi_k = \xi_0^k h + \sum_{l=1}^{\infty} \xi_l^k \omega_{l-1} . \quad (11)$$

Using the hermiticity of the mass matrix, we can invert this relation to derive the relations between h and the ω_k in terms of the mass eigenstates

$$h = \sum_{l=0}^{\infty} \xi_0^l \phi_l \quad , \quad \omega_k = \sum_{l=0}^{\infty} \xi_{k+1}^l \phi_l . \quad (12)$$

From Eq. (12), it is clear that the SM fields couple to the physical fields just like they would couple to the SM Higgs boson, but with a factor ξ_0^l for each ϕ_l leg at the vertex. As the couplings among the scalar fields are slightly more complicated, we have moved the detailed Feynman rules to Appendix A 3.

According to Eq. (1), Eq. (5) and Eq. (6), the model can be parameterized by the SM parameters m_h and v together with the bulk mass m_b , the trilinear coupling g^2 and the compactification scale R^{-1} , which is the parameterization that we will adopt for the rest of this work. However, let us note that, while v at tree level has the usual relation to the mass of the W boson m_W ,

$$v = 2 \frac{m_W \sin \theta_W}{e} ,$$

with θ_W being the weak mixing angle and e the electromagnetic coupling, m_h generally does not coincide with any of the masses of the physical scalar modes.

On closer examination of the scalar spectrum, two very different cases can be distinguished and are shown in Fig. 1 where $|\xi_0^k|$ (which controls the couplings to the SM particles) is displayed as a function of the mass of the modes⁴. If m_h lies below m_b (left hand side of

⁴ These figures are closely related to the Källén-Lehmann spectral density of h which is given by $\rho(s) = \sum_{k=0}^{\infty} (\xi_0^k)^2 \delta(s - \lambda_k^2)$.

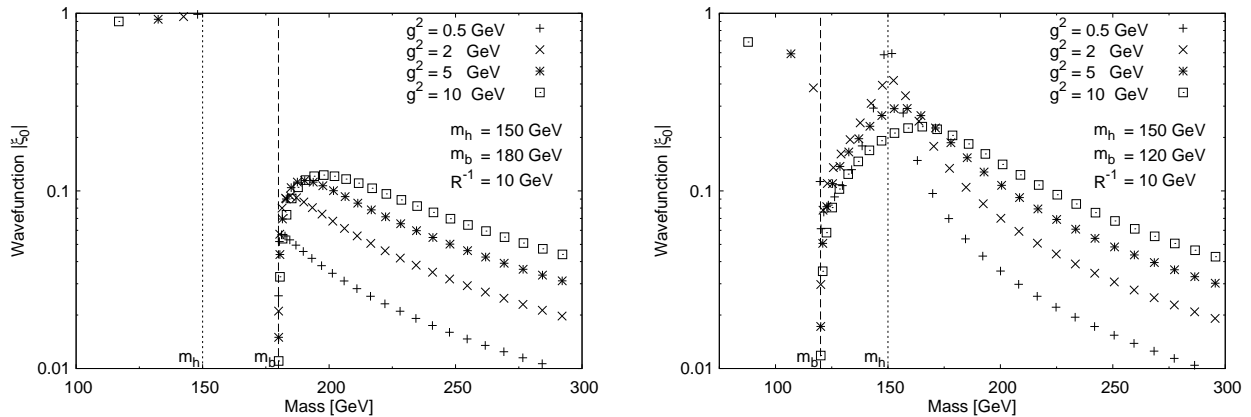


FIG. 1: Compact HEIDI spectra for the two different scenarios referred to in the text below. The respective values of m_h and m_b are marked with vertical lines.

Fig. 1), we find that the lightest mode, which always lies below m_b as argued above, has $|\xi_0^0|$ close to one. The other modes form a tower starting at m_b with the couplings of this “would-be continuum” being smaller by about an order of magnitude and dropping off for higher masses. Increasing g^2 pushes the mass of the lowest mode towards zero and enhances the couplings of the would-be continuum, while the mass of the lowest mode approaches m_h in the limit $g^2 \rightarrow 0$ with $|\xi_0^0| \rightarrow 1$, and the other modes decouple from the SM.

If m_h lies above m_b (right hand side of Fig. 1), the situation looks similar for large values of g^2 . However, if we decrease this parameter, the lightest mode moves towards m_b with its coupling to the SM decreasing. At the same time, a peak in the would-be continuum is appearing at m_h . In the limit $g^2 \rightarrow 0$, this peak evolves into a single mode with a SM coupling of one, while the other modes (this time including the lowest one) decouple.

For both cases, the asymptotic spacing between the modes is given by the compactification scale R^{-1} . In the limit of large R , the modes in the would-be continuum approach each other, while their couplings to the SM go to zero.

C. Considerations regarding simulations

A thorough study of the phenomenology of compact HEIDI requires its implementation into an event generator and the simulation of the different Higgs production channels within the HEIDI scenario. Considering that all relevant processes feature at least a four-particle final state already at the parton level and taking into account that the number of Feynman diagrams is multiplied by the number of propagating scalar fields, speed is a critical issue here. Therefore, as the parton-level event generator WHIZARD [6, 7] can handle final states with six to eight particles in the SM and in the Minimal Supersymmetric Standard Model (MSSM) [8–10], and has been used especially for many alternative models of EWSB [11–14], it is a good choice for the investigation of compact HEIDI models as well.

For the actual implementation of the model, the tower of scalar fields must be truncated at a cutoff scale Λ . However, if we choose the bulk mass m_b to be of the order of the weak scale and R^{-1} is small, then it is easy to see from Eq. (10) that the spectrum will contain a large number of scalar fields below Λ . As a consequence, even though at the Lagrangian level the HEIDI model is a straightforward deformation of the scalar sector of

the SM, consisting of the simple addition of a single five-dimensional scalar singlet, the implementation of the model into WHIZARD (as well as into any other matrix element generator) will result in the addition of a very large number of particles and interactions to the existing SM implementation of the code. In addition, the number of fields below the cutoff depends on the parameters of the model. We therefore choose to follow the approach introduced in Ref. [16] and implement the model using the newly developed FEYNRULES interface to WHIZARD [17]. In the next section we briefly outline some of the details of the implementation using that interface.

III. PREREQUISITES FOR SIMULATION

In this section we describe the implementation of the compact HEIDI model of Section II into FEYNRULES. We first explain how the numeric spectrum and widths of the scalar fields are obtained for a given point in parameter space, while the actual FEYNRULES implementation is presented afterwards. The FEYNRULES model files are available for download from the FEYNRULES model database located at

<https://server06.fynu.ucl.ac.be/projects/feynrules/wiki/ModelFiles>

A. Spectrum and widths

According to Eq. (9), the masses λ_k of the physical scalar modes are encoded as the zeroes of a transcendental function $f(\lambda_k^2)$. As no analytic expression for these roots exists, a procedure for their numerical determination is necessary.

As has already been observed in Section II A, the lowest mode is always located in the interval between 0 and m_b , and the would-be continuum which starts at m_b has exactly one mode in each of the intervals of Eq. (10). As $f(\lambda^2)$ is monotonous between the boundaries of the intervals, it is possible to calculate the masses by the bisection method: for each mode, we start in the middle of the respective interval and then, depending on the sign of f , split the interval we know to contain a root in two until sufficient precision has been reached. This is guaranteed to find all modes, starting from the lowest one.

Once the mass of a mode λ_k has been determined, the mixing parameters ξ_i^k defined in Eq. (11) can be calculated as functions of λ_k through application of Eq. (A11) and Eq. (A13). From the mixing parameters, the trilinear and quartic scalar self-couplings can be derived according to the Feynman rules given in Appendix A 3. We have implemented the calculation of the masses, mixings and self-couplings into a spectrum calculator. While this is included in the model file for FEYNRULES, it is also available as a stand-alone MATHEMATICA package.

In addition to masses and couplings, the widths of the scalar modes are required for simulating collider cross sections. As the couplings of the ϕ_k to the SM particles are identical to the respective Higgs couplings up to factors of ξ_0^k (*cf.* Appendix A 3), their decay widths into SM particles can be approximated⁵ by the corresponding Higgs widths, scaled by factors of $|\xi_0^k|^2$. We have chosen to take the necessary SM Higgs width from HDECAY [18]. In order to avoid a run-time dependence on the HDECAY package, we have parametrized the Higgs

⁵ There is a small correction coming from diagrams involving both SM particles and other scalar fields ϕ_k .

mass dependence of its output in a dedicated MATHEMATICA module (which is also contained within the FEYNRULES model file). As the presence of thresholds spoils any simple ansatz for fitting, we parameterize the width by a grid of 100 points for Higgs masses below 500 GeV (with linear interpolation between the grid points), while an interpolating polynomial of degree 6 is used above 500 GeV. Comparison shows that the result approximates the corresponding HDECAY output well at least up to 4 TeV.

Using this parameterization, our spectrum calculator is able to automatically determine the widths of the HEIDI scalar fields. In addition to the aforementioned decays into SM particles, two body decays into two scalar modes are also included into the calculation.

B. FEYNRULES implementation

Since the multi-scalar couplings are only of small phenomenological relevance and at the same time slow down both FEYNRULES and the matrix element generator considerably (their number growing combinatorically with the number of modes), we restrict the implementation to the SM sector of the model. To this end, we insert Eq. (12) into the SM Lagrangian and induce in this way the coupling between the HEIDI modes ϕ_k and the SM fermions and vector bosons, which is enough to study most of the LHC phenomenology of this model. In addition, we restrict the implementation to unitarity gauge. In the rest of this section we describe the FEYNRULES implementation of the model which is special in the sense that the number of modes below the cutoff and thus the number of particles in the model is variable.

Since the compact HEIDI model consists of the SM to which we add the HEIDI sector, the FEYNRULES implementation can be achieved in a natural way by extending the already existing implementation of the SM in FEYNRULES, contained in the file `SM.fr` included in the FEYNRULES distribution. In this process⁶, `SM.fr` can remain unchanged, and the new model file only has to encode the new parameters, fields and the modified SM Lagrangian.

Before the spectrum of the model can be calculated, the Higgs vacuum expectation value v and its pre-mixing mass m_h , the bulk mass m_b , the HEIDI coupling g^2 and the compactification scale R^{-1} must be specified (*cf.* Section II A). In addition, for the actual implementation, we need to truncate the infinite tower of Kaluza-Klein states to a finite number by choosing a cutoff scale Λ . These six parameters, which must be known *before* any code for a matrix element generator can be emitted, have been implemented as a set of flags which must be specified before the model can be loaded successfully and which are listed in Tab. I. It is important to realize that those values are hardcoded in the generated model files. In particular, the electroweak scale implied by the runtime input parameters *must* match the value of v set by the aforementioned flags.

After setting the flags from Tab. I, the model such defined can be loaded into FEYNRULES and the WHIZARD interface can be invoked as described in [17].

⁶ As the SM Higgs field h is no longer a mass eigenstate in the model, it can be removed from the set of physical fields by adding `Unphysical -> True` to its definition in `SM.fr`. However, this step is strictly optional and no harm is done by omitting it.

Flag	Description
HEIDI\$v	SM Higgs boson vev
HEIDI\$mh	SM Higgs mass
HEIDI\$cs	compactification scale R^{-1}
HEIDI\$mb	bulk mass m_b
HEIDI\$g2	5D trilinear coupling squared
HEIDI\$cutoff	cutoff scale Λ
HEIDI\$nmodes	Number of HEIDI modes below the cutoff scale Λ (determined automatically if HEIDI\$cutoff is set)

TABLE I: The flags in the FEYNRULES implementation of the compact HEIDI model which must be set before the model can be used.

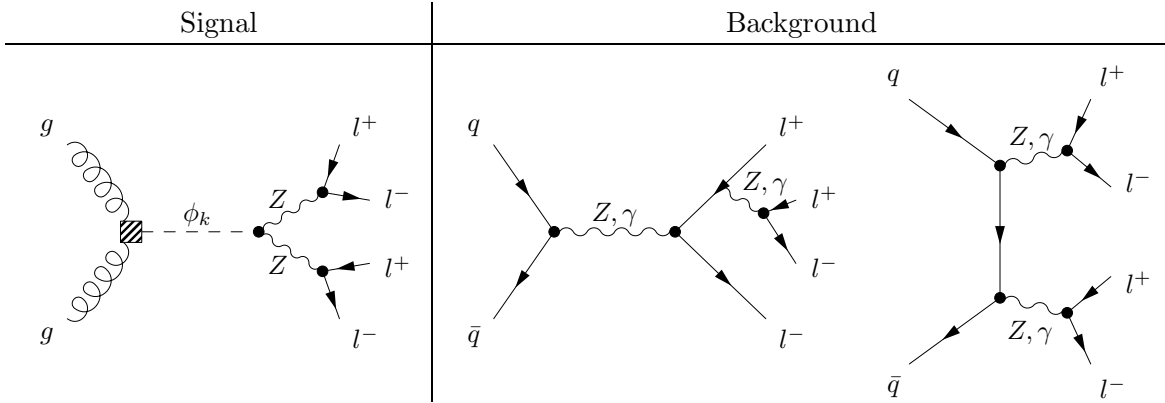


FIG. 2: Diagrams contributing to signal and background for scalar particle production in $pp \rightarrow ZZ \rightarrow 4l$. The shaded box represents the effective gluon fusion operator obtained from integrating out the top quark.

IV. HEIDI SCALARS IN THE GOLDEN CHANNEL AT THE LHC

In order to study the impact of HEIDI on one of the major Higgs search channels at the LHC, we have performed simulations of scalar particle production in gluon fusion with the subsequent decay into four leptons via two virtual Z bosons, the so-called golden channel for Higgs discovery at the LHC. As gluon fusion is a loop induced process with the dominant contribution at leading order coming from the top quark triangle, we have added to the Lagrangian the corresponding operator obtained by integrating out the top quark (*cf.* Appendix A 4).

At lowest order in the strong coupling, the signal in this process is mediated by gluon initiated s -channel type diagrams such as the one shown in Fig. 2 left, while the background processes always have quarks in the initial state and consist of diagrams such as those in Fig. 2 right. Therefore, a significant part of the background is contributed by processes with a valence and a sea quark in the initial state. As those processes tend to be more strongly boosted when compared to processes initiated by sea quarks or by gluons, it is possible to remove part of the background by a cut on the total rapidity. We thus chose to apply a cut of

$$|y| \leq 2$$

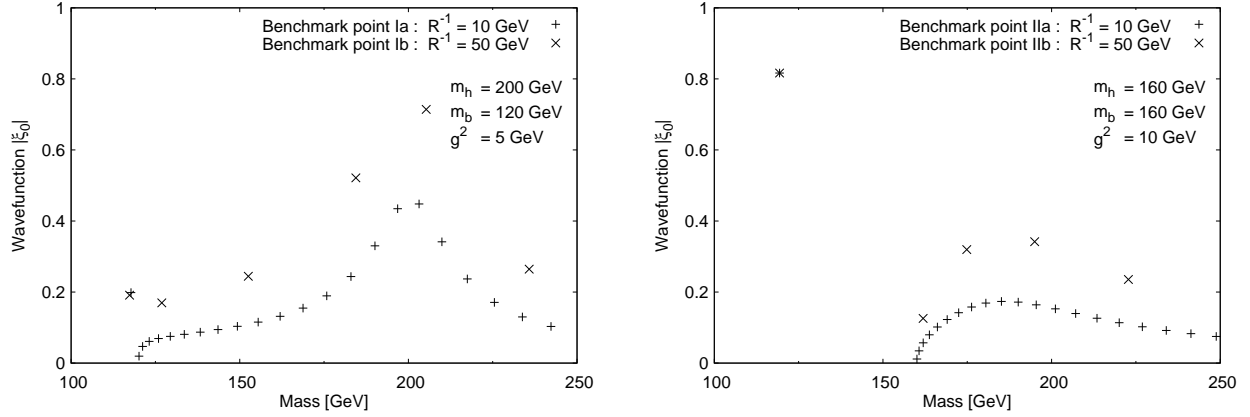


FIG. 3: The scalar field spectra at the four benchmark points at which simulations have been performed.

on the total rapidity of the final state.

Additional background can be removed by cutting the invariant mass of the leptons to the Z mass window. However, as we do not want to lose sensitivity to the scalar modes which lie below the pair production threshold, we must allow for lepton pairs with invariant mass significantly below the Z mass and therefore have enforced the cut

$$10 \text{ GeV} \leq m_{ll} \leq 100 \text{ GeV}$$

on the invariant mass of the lepton pairs. If the final state consists of four leptons of the same generation, we demanded that at least one of the two possible combinations satisfies the cut. In order to account for detector acceptance and for the fact that we require four separately resolved leptons, we have applied a p_T cut as well as cuts on the angular separation and on the polar angle of the leptons

$$p_T > 5 \text{ GeV} \quad , \quad |\cos \theta_{ll}| \leq 0.99 \quad , \quad |\cos \theta_l| \leq 0.99 \quad .$$

We have performed simulations at four different benchmark points in parameter space which are shown in Fig. 3. The parameter sets Ia and Ib differ only by the compactification scale and have $m_h = 200 \text{ GeV}$ and $m_b = 120 \text{ GeV}$. As discussed in Section II B, this implies that the would-be SM Higgs boson corresponds to a bump in the would-be continuum around m_h as clearly visible in the spectra shown in Fig. 3 left. At point Ia, the compactification scale is $R^{-1} = 10 \text{ GeV}$ with more than 20 modes lying below 250 GeV, while we only have 6 such modes at Ib with $R^{-1} = 50 \text{ GeV}$, their couplings to the SM particles being enhanced in exchange.

At IIa and IIb, we set $m_h = m_b = 160 \text{ GeV}$. As discussed in Section II B and clearly visible from Fig. 3 on the right, the spectrum is very different in this case, with the lowest mode corresponding to the would-be Higgs boson, and the couplings of the would-be continuum to the SM being strongly suppressed. Again, we chose $R^{-1} = 10 \text{ GeV}$ for IIa and $R^{-1} = 50 \text{ GeV}$ for IIb.

For the actual simulation, we took the first two quark generations and gluons into account as potential initial particles, simulated the full $2 \rightarrow 4$ processes using the CTEQ6L [19] series of parton distribution functions and generated unweighted events for an integrated luminosity of 100 fb^{-1} at $\sqrt{s} = 14 \text{ TeV}$. As the background is the same for all four benchmark

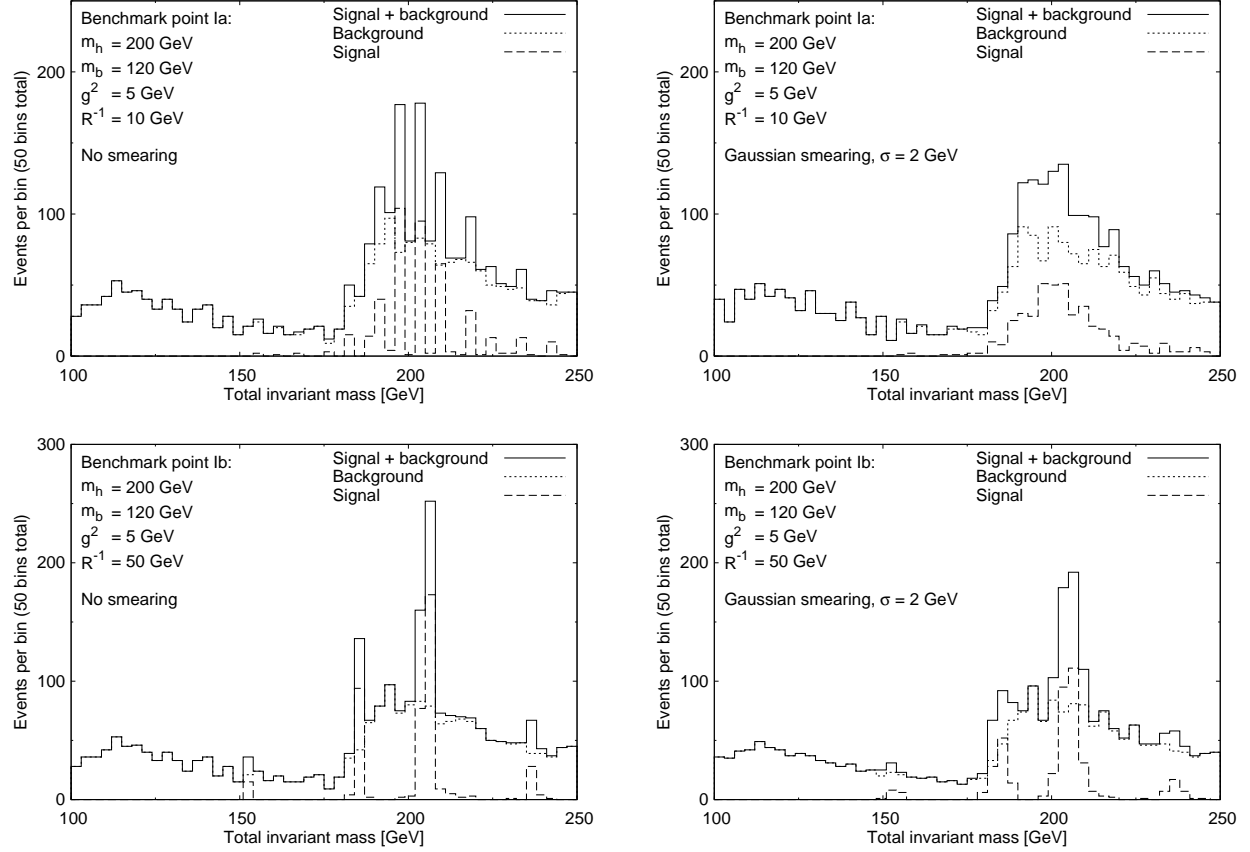


FIG. 4: Total invariant mass distributions in $pp \rightarrow 4l$ at benchmark points Ia and Ib. For the distributions in the right column, a Gaussian smearing with $\sigma = 2$ GeV has been applied to the invariant mass in order to simulate measurement errors.

points, we generated a single set of background events, while a fresh set of signal events was generated for each point.

The top left panel of Fig. 4 shows the resulting invariant mass distribution for benchmark point Ia. Despite the fact that the scalar field tower already starts at 120 GeV, the actually visible resonances only start at the Z pair production threshold, demonstrating that the SM couplings of those modes are much too small to win over the suppression coming from the off-shell Z propagators. Above the threshold, the comblike structure coming from the scalar resonances is clearly visible not only in the actual signal, but persists also when the background is added.

The same distributions are shown in the top right panel of Fig. 4, but now with a Gaussian smearing with standard deviation $\sigma = 2$ GeV applied to the invariant mass in order to simulate a measurement error. Although the width of the Gaussians is still significantly smaller than the average mode spacing of about 10 GeV, the histogram shows that this is already enough to destroy the comblike structure of the would-be continuum. What remains is a broad excess above the background which peaks around m_h and resembles a single, very broad resonance.

The bottom panels of Fig. 4 show the unsmeared (left) and smeared (right) distributions for benchmark point Ib. As detailed above, the only difference with point Ia is the larger spacing of the individual modes and the therefore enhanced couplings to the SM. Before

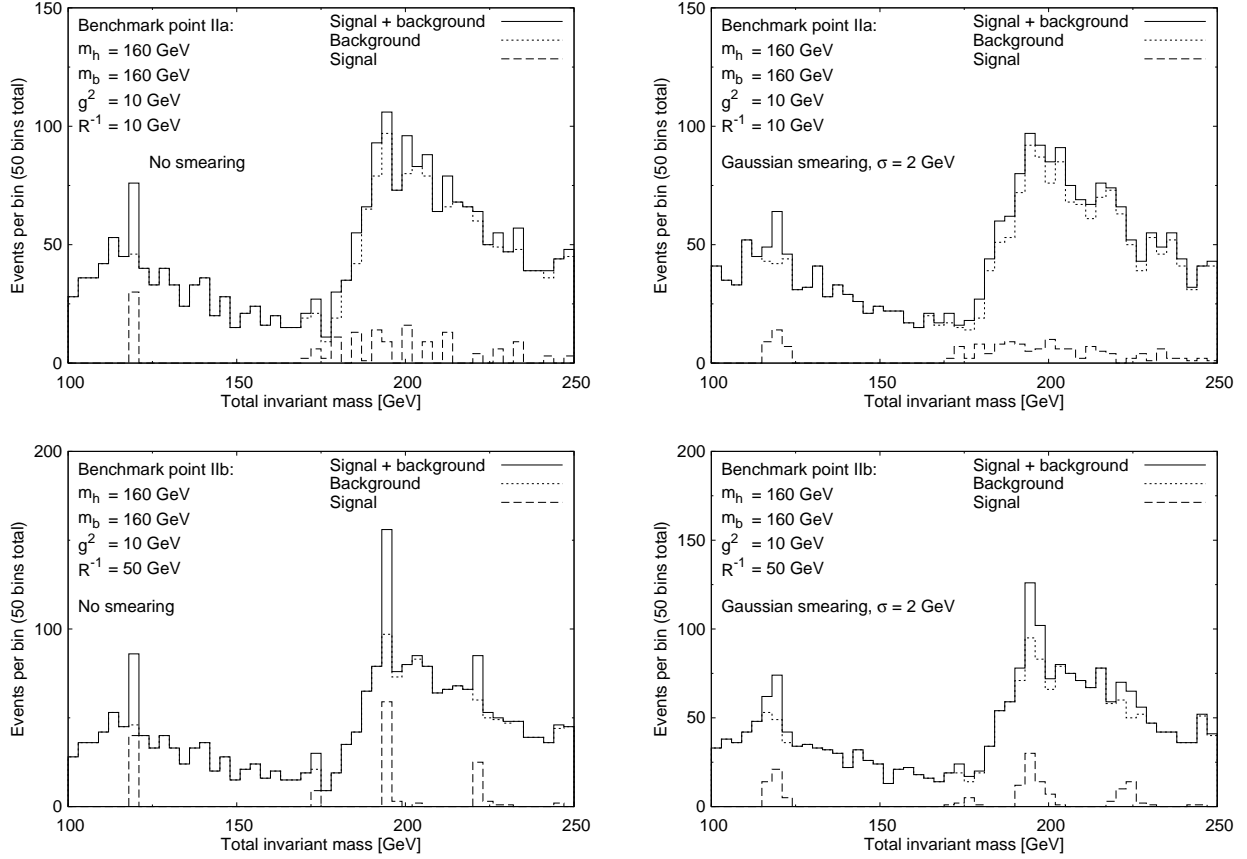


FIG. 5: Like Fig. 4, but for the benchmark points IIa and IIb.

the smearing is applied, four modes are visible in the signal (one of them below the Z pair threshold with a mass of ≈ 150 GeV), and the three heaviest of them also stick out above the background. While the smearing distorts the shape of the peaks and makes them less pronounced, the smeared peaks are still visible above the background.

In the same way, the invariant mass distributions for benchmark points IIa and IIb are shown in Fig. 5, the top panels again showing the case with the smaller mode spacing. The different structure of the spectrum discussed above also manifests itself in the distributions. The lowest mode, which again lies at about 120 GeV, has nearly SM-like couplings in this scenario and is therefore a prominent feature in the signal distribution. Despite lying far below the Z pair threshold, the corresponding peak is more than comparable in size with the peaks from the would-be continuum. After adding the background, the lowest mode still sticks out and remains visible, while the comblike structure of the other modes is masked by the background fluctuations with only a diffuse excess being observable. Applying the smearing degenerates the peak of the lowest mode and homogenizes the (small) excess over the background.

The distributions for benchmark point IIb again differ by the mode count. While the appearance of the lowest mode is virtually identical to scenario IIa (as is clear from Fig. 3), the would-be continuum now exhibits two moderate peaks in the signal, both of which survive when the background is added. After the smearing is added, at least one of those two peaks remains visible over the background together with the lowest mode.

Our simulations show that the model could, depending on the scenario realized, appear in very different guises, ranging from a Higgs-like peak with reduced magnitude and a diffuse continuum (IIa), a series of sharp resonances (IIb and Ib) or a single, very broad excess (Ia). At least for Ia / Ib, the signal is clearly visible over the background and a discovery might be possible in this channel. For IIb and especially IIa, the situation looks more pessimistic; especially in IIa where the diffuse shape of the signal might get lost in the background. However, while being the first detailed exploration of a HEIDI-like scalar sector at the LHC, our simulations are still too simplistic to make realistic efficiency estimates for a discovery. To this end, a more detailed study of the background and of higher order corrections is required as well as the inclusion of other potential discovery channels like gauge boson fusion and “HEIDI strahlung”. We postpone this to a future publication.

V. CONCLUSIONS

In this paper, we have presented a first study of the LHC phenomenology of an extended scalar sector built from a compact extra dimension, where the SM fields are living on a brane and only a single singlet scalar field is allowed to propagate in the bulk. This is a representative of a class of models known as higher-dimensional (“HEIDI”) Higgs models.

Despite the presence of just a single higher-dimensional scalar singlet, the physics and phenomenology of this model is astonishingly rich. The main effect comes from the Kaluza-Klein tower of scalar resonances mixing with the SM Higgs scalar field. As the extra-dimensional scalar fields couple to SM particles through this mixing, the SM Higgs boson gets diluted to a tower of scalar fields of ascending mass whose couplings to the SM particles are reduced significantly compared to the SM Higgs boson.

We concentrated on the so-called “golden channel” for a not too light Higgs boson decaying predominantly into two Z bosons, the latter decaying into four leptons, and restricted ourselves to the gluon-fusion production channel. Our main results in Section IV show a variety of different shapes which such a model could produce, depending on the point in parameter space under consideration. These shapes range from a simple reduction of a SM Higgs signal with a diffuse continuum tail to a series of Kaluza-Klein peaks to a very broad continuous bump, showing the phenomenological richness of these otherwise simple extensions of the SM. While this phenomenological variety is a generic property of the model which derives from its spectrum, it would certainly be interesting to see how the other classic Higgs production channels perform for this type of model. We conclude by remarking that even a rather trivial deformation of the SM in the scalar sector can have the potential to jeopardize the common assumption that the LHC cannot fail in its mission to discover either the Higgs boson or new physics.

Acknowledgments

CS has been supported by the Deutsche Forschungsgemeinschaft through the Research Training Groups GRK 1147 *Theoretical Astrophysics and Particle Physics* and GRK 1102 *Physics of Hadron Accelerators*. JRR has been partially supported by the Ministry of Science and Culture (MWK) of the German state Baden-Württemberg. BF acknowledges support by the Theory-LHC France-initiative of the CNRS/IN2P3. NDC was supported by the US National Science Foundation under grants PHY-0354226 and PHY-0705682. We are also

indebted to J. van der Bij for many instructive discussions on the nature of HEIDI-type models.

Appendix A: Diagonalizing compact HEIDI

1. Vacuum expectation values

From Eq. (1) and Eq. (3), we can read off the classical potential for the vacuum expectation values of the fields Eq. (4),

$$V(v, w) = \frac{1}{4}\lambda v^4 - \frac{1}{2}\mu^2 v^2 + \underbrace{\sum_{k=0}^{\infty} \left(\frac{1}{2}m_k^2 w_k^2 - \frac{g}{N_k \sqrt{R}} v^2 w_k \right)}_{V_k(v, w_k)}. \quad (\text{A1})$$

For any fixed value of v , Eq. (A1) decomposes into a constant term plus a sum of second degree polynomials V_k , each depending only on a single w_k . If we have $m_b > 0$, then each of the V_k is bounded from below, and the minima are given by

$$w_k = \frac{g}{N_k \sqrt{R} m_k^2} v^2. \quad (\text{A2})$$

Therefore, the potential V is always bounded from below as a function of the w_k for fixed v and $m_b > 0$, and inserting Eq. (A2) into Eq. (A1) gives the minimum

$$V_0(v) = \frac{1}{4}(\lambda - \alpha) v^4 - \frac{1}{2}\mu^2 v^2. \quad (\text{A3})$$

With the help of

$$\sum_{k=0}^{\infty} \frac{1}{1 + \frac{k^2}{x^2}} = \frac{1}{2} + \frac{\pi x}{2} \coth(\pi x), \quad (\text{A4})$$

α in Eq. (A3) can be written as

$$\alpha = \frac{g^2}{R} \sum_{k=0}^{\infty} \frac{1}{N_k^2 m_k^2} = \frac{g^2}{m_b} \coth(R\pi m_b). \quad (\text{A5})$$

In order to derive the conditions under which Eq. (A1) is bounded from below as a function of both v and the w_k , it is sufficient to examine the asymptotic behavior of Eq. (A3) which is determined by the sign of the quartic term. As α can be easily seen to be positive definite from Eq. (A5), we end up with four different scenarios:

1. $\mu^2 > 0$, $\lambda > \alpha$:

V is bounded from below and has two minima at

$$v = \pm \frac{\mu}{\sqrt{\lambda - \alpha}} , \quad w_k = \frac{g}{N_k \sqrt{R} m_k^2} v^2. \quad (\text{A6})$$

The point $v = w_k = 0$ is unstable.

2. $\mu^2 > 0$, $\lambda \leq \alpha$:
The potential is not bounded.
3. $\mu^2 \leq 0$, $\lambda \geq \alpha$:
 V is bounded from below and has a single minimum at $v = w_k = 0$
4. $\mu^2 \leq 0$, $\lambda < \alpha$:
The potential is not bounded.

Therefore, we need $\mu^2 > 0$ and $\lambda > \alpha$ in order to have a stable theory with spontaneous symmetry breaking. The two solutions Eq. (A6) are equivalent and only differ by a field redefinition $h \rightarrow -h$ as can be seen from Eq. (7), and we therefore are free to make the choice Eq. (5).

2. Mass eigenstates and wave functions

Arranging the fields h and ω_k into the vector

$$\Upsilon = (h, \omega_0, \omega_1, \dots)^T$$

and introducing the mass matrix M

$$(M\Upsilon)_k = \begin{cases} m_h^2 h + \sum_{l=0}^{\infty} \rho_l \omega_l & \text{for } k = 0 \\ \rho_{k-1} h + m_{k-1}^2 \omega_{k-1} & \text{for } k > 0 \end{cases} \quad (\text{A7})$$

with the abbreviation

$$\rho_k = \frac{2gv}{N_k \sqrt{R}} ,$$

the mass and mixing terms in Eq. (7) can be written as

$$-\frac{1}{2} m_h^2 h^2 - \sum_{k=0}^{\infty} \left(\frac{1}{2} m_k^2 \omega_k^2 - \frac{2gv}{N_k \sqrt{R}} h \omega_k \right) = -\frac{1}{2} \Upsilon^T M \Upsilon .$$

In order to find the eigenvalues λ_k^2 to the eigenvectors⁷

$$\xi^k = (\xi_0^k, \xi_1^k, \dots)^T , \quad M \xi^k = \lambda_k^2 \xi^k , \quad (\text{A8})$$

we rewrite the eigenvalue condition of Eq. (A8) in terms of the components ξ_i^k

$$\lambda_k^2 \xi_0^k = m_h^2 \xi_0^k + \sum_{i=0}^{\infty} \rho_i \xi_{i+1}^k , \quad (\text{A9})$$

$$\lambda_k^2 \xi_i^k = \rho_{i-1} \xi_0^k + m_{i-1}^2 \xi_i^k \quad \text{for } i > 0 . \quad (\text{A10})$$

⁷ Note that this definition of the ξ_i^k is equivalent to that given in Eq. (11).

Since assuming $\xi_0^k = 0$ and $\xi_i^k \neq 0$ for some $i > 0$ leads to a contradiction, we can therefore solve Eq. (A10) in terms of ξ_0^k ,

$$\xi_i^k = \xi_0^k \frac{\rho_{i-1}}{\lambda_k^2 - m_{i-1}^2} . \quad (\text{A11})$$

Upon inserting Eq. (A11) into Eq. (A9), ξ_0^k drops out and application of Eq. (A4) finally leads to the result Eq. (9). In order to obtain the normalized eigenvectors ξ^k , we rewrite the normalization condition using Eq. (A11)

$$1 = \sum_{i=0}^{\infty} (\xi_i^k)^2 = (\xi_0^k)^2 \left(1 + \sum_{i=0}^{\infty} \left(\frac{\rho_i}{\lambda_k^2 - m_i^2} \right)^2 \right) . \quad (\text{A12})$$

The sums appearing in Eq. (A12) can be performed analytically, and solving this equation for ξ_0^k , one obtains,

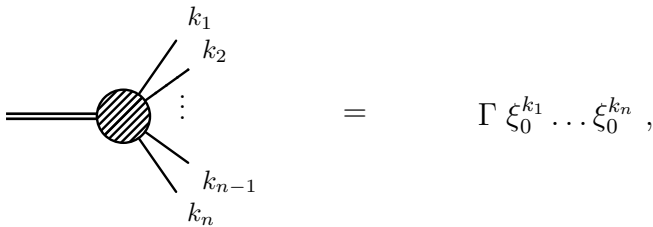
$$(\xi_0^k)^{-2} = 1 + \frac{g^2 v^2 R \pi}{\lambda_k^2 - m_b^2} + \frac{1}{2} \frac{\lambda_k^2 - m_h^2}{\lambda_k^2 - m_b^2} + \frac{R \pi}{4 g^2 v^2} (\lambda_k^2 - m_h^2)^2 . \quad (\text{A13})$$

The other components of the eigenvectors can be derived by inserting Eq. (A13) into Eq. (A11).

3. Feynman rules

As the model differs from the SM in the scalar sector only, all couplings involving fermions and gauge bosons are unchanged and need not be repeated here. To obtain the Feynman rules involving the scalar fields, we have to take the full Lagrangian of the model (which consists of the SM Lagrangian together with the scalar sector Eq. (7)) and express h and the ω_k through the mass eigenstates ϕ_k by application of Eq. (12).

For the couplings between the ϕ_k and the SM vectors and fermions, the resulting Feynman rules are trivially obtained by taking the SM rules and replacing the Higgs legs with the ϕ_k , multiplying with a factor ξ_0^k for every scalar leg. The results are Feynman rules which look like



$$\text{Diagram} = \Gamma \xi_0^{k_1} \dots \xi_0^{k_n} ,$$

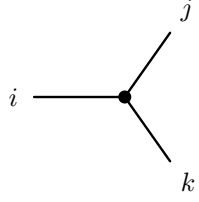
where the double line represents all vector and fermion lines, and Γ is the SM vertex factor (including the color and Lorentz structures).

The trilinear scalar couplings are more complicated: the piece of Eq. (7) which encodes them is

$$\mathcal{L}_3 = -\lambda v h^3 + \sum_{k=0}^{\infty} \frac{g}{N_k \sqrt{R}} h^2 \omega_k .$$

To obtain the corresponding Feynman rule in a compact form, we insert the physical fields via Eq. (12), sum the series using Eq. (A11) and Eq. (A4), apply Eq. (9) and replace λ

using Eq. (6). We eventually derive



$$= \frac{i}{v} \xi_0^i \xi_0^j \xi_0^k (\lambda_i^2 + \lambda_j^2 + \lambda_k^2 - 6m_h^2) .$$

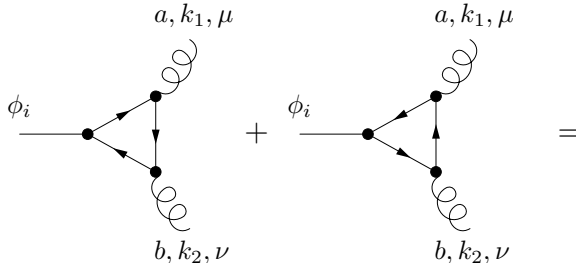
The quartic couplings are considerably simpler to obtain since it is sufficient to insert Eq. (12) into the h^4 term of Eq. (7). We directly get



$$= -i3!\lambda \xi_0^i \xi_0^j \xi_0^k \xi_0^l .$$

4. The effective scalar-gluon-gluon coupling

Straightforward evaluation of the matrix element for on-shell gluon fusion of a single scalar mode ϕ_i via a top quark loop gives (*cf.* [22])



$$= \frac{\alpha_s}{8\pi v} \xi_0^i \tau_i \underbrace{(1 + (1 - \tau_i) g(\tau_i))}_{\rho(\tau_i)} (k_1^\nu k_2^\mu - g^{\mu\nu} (k_1 k_2)) \delta_{ab} \quad (\text{A14})$$

where the function $g(\tau)$ is defined piecewise as

$$g(\tau) = \begin{cases} \arcsin^2 \sqrt{\frac{1}{\tau}} & \text{for } \tau \geq 1 \\ -\frac{1}{4} \left(\log \left(\frac{1+\sqrt{1-\tau}}{1-\sqrt{1-\tau}} \right) - i\pi \right)^2 & \text{for } \tau < 1 \end{cases}$$

and τ_i is defined as

$$\tau_i = 4 \frac{m_t^2}{\lambda_i^2}$$

with the top quark mass m_t and the scalar field mass λ_i . The amplitude Eq. (A14) is reproduced by the trilinear part of the gauge-invariant effective operator

$$\mathcal{O}_{gg\phi} = \sum_{i=0}^{\infty} \frac{\alpha_s}{16\pi v} \xi_0^i \rho(\tau_i) \phi_i \text{tr} G_{\mu\nu} G^{\mu\nu} \quad (\text{A15})$$

with the gluon field strength tensor $G^{\mu\nu}$.

The scalar ϕ_i can be taken off the mass shell simply by replacing λ_i^2 by its momentum p^2 , and the lowest order of the expansion of Eq. (A14) in p^2 can then be obtained by taking the limit

$$\lim_{\tau \rightarrow \infty} \rho(\tau) = \frac{2}{3}$$

Inserting this limit into Eq. (A15), we obtain the lowest dimension operator contributing to gluon fusion in the effective theory obtained by consistently integrating out the top quark

$$\mathcal{O}_{gg\phi}^0 = \sum_{i=0}^{\infty} \frac{\alpha_s}{24\pi v} \xi_0^i \phi_i \text{tr} G_{\mu\nu} G^{\mu\nu} \quad (\text{A16})$$

Both effective operators are available in our FEYNRULES HEIDI implementation via the function `LHEIDIgg`. Calling this function as `LHEIDIgg["heavytop"]` generates Eq. (A16), while Eq. (A15) can be obtained by omitting the argument. For the simulation results presented in this work, Eq. (A16) has been used.

-
- [1] J. J. van der Bij, Phys. Lett. B **636**, 56 (2006) [arXiv:hep-ph/0603082].
 - [2] J. J. van der Bij and S. Dilcher, Phys. Lett. B **655**, 183 (2007) [arXiv:0707.1817 [hep-ph]].
 - [3] J. J. van der Bij and B. Pulice, Nucl. Phys. B **853**, 49 (2011) [arXiv:1104.2062 [hep-ph]].
 - [4] J. J. van der Bij, arXiv:1204.3435 [hep-ph].
 - [5] A. Hill and J. J. van der Bij, Phys. Rev. D **36**, 3463 (1987).
 - [6] W. Kilian, T. Ohl and J. Reuter, Eur. Phys. J. C **71**, 1742 (2011) [arXiv:0708.4233 [hep-ph]].
 - [7] M. Moretti, T. Ohl and J. Reuter, arXiv:hep-ph/0102195.
 - [8] K. Hagiwara *et al.*, Phys. Rev. D **73**, 055005 (2006) [arXiv:hep-ph/0512260].
 - [9] J. Kalinowski, W. Kilian, J. Reuter, T. Robens and K. Rolbiecki, JHEP **0810**, 090 (2008) [arXiv:0809.3997 [hep-ph]].
 - [10] T. Robens, J. Kalinowski, K. Rolbiecki, W. Kilian and J. Reuter, Acta Phys. Polon. B **39**, 1705 (2008) [arXiv:0803.4161 [hep-ph]].
 - [11] T. Ohl and C. Speckner, Phys. Rev. D **78**, 095008 (2008) [arXiv:0809.0023 [hep-ph]].
 - [12] W. Kilian, D. Rainwater and J. Reuter, Phys. Rev. D **74**, 095003 (2006) [arXiv:hep-ph/0609119].
 - [13] M. Beyer, W. Kilian, P. Krstonsic, K. Monig, J. Reuter, E. Schmidt and H. Schroder, Eur. Phys. J. C **48**, 353 (2006) [arXiv:hep-ph/0604048].
 - [14] W. Kilian, D. Rainwater and J. Reuter, Phys. Rev. D **71**, 015008 (2005) [arXiv:hep-ph/0411213].
 - [15] N. D. Christensen and C. Duhr, Comput. Phys. Commun. **180**, 1614 (2009) [arXiv:0806.4194 [hep-ph]].
 - [16] N. D. Christensen *et al.*, arXiv:0906.2474 [hep-ph].
 - [17] N. D. Christensen, C. Duhr, B. Fuks, J. Reuter and C. Speckner, Eur. Phys. J. C (in print), arXiv:1010.3251 [hep-ph].
 - [18] A. Djouadi, J. Kalinowski and M. Spira, Comput. Phys. Commun. **108**, 56 (1998) [arXiv:hep-ph/9704448].
 - [19] J. Pumplin, D. R. Stump, J. Huston, H. L. Lai, P. M. Nadolsky and W. K. Tung, JHEP **0207**, 012 (2002) [arXiv:hep-ph/0201195].
 - [20] M. R. Whalley, D. Bourilkov and R. C. Group, arXiv:hep-ph/0508110.
 - [21] T. Ohl, Comput. Phys. Commun. **120**, 13 (1999) [arXiv:hep-ph/9806432].
 - [22] J. F. Gunion, H. E. Haber, G. L. Kane and S. Dawson, *The Higgs Hunter's guide*, and references therein.